Biomedicine & Pharmacotherapy 153 (2022) 113428

Contents lists available at ScienceDirect

Biomedicine & Pharmacotherapy

journal homepage: www.elsevier.com/locate/biopha

PCSK9 conjugated liposomes for targeted delivery of paclitaxel to the cancer cell: A proof-of-concept study

Nitin Bharat Charbe [a,b,*], Carlos F. Lagos [c], Cristian Andrés Vilos Ortiz [d], Murtaza Tambuwala [e,f,**], Sushesh Srivatsa Palakurthi [b], Flavia C. Zacconi [a,g,*]

[a] Departamento de Química Orgánica, Facultad de Química y de Farmacia, Pontificia Universidad Católica de Chile, Av. Vicuña McKenna 4860, 7820436, Macul, Santiago, Chile
[b] Department of Pharmaceutical Sciences, Irma Lerma Rangel College of Pharmacy, Texas A&M University, USA
[c] Chemical Biology & Drug Discovery Lab, Facultad de Medicina y Ciencia, Universidad San Sebastián, Campus Los Leones, Lota 2465 Providencia 7510157, Santiago, Chile
[d] Laboratory of Nanomedicine and Targeted Delivery, Center for Medical Research, School of Medicine, Universidad de Talca, Talca, Chile
[e] SAAD Centre for Pharmacy and Diabetes, School of Pharmacy and Pharmaceutical Science, Ulster University, Coleraine, County Londonderry, Northern Ireland BT52 1SA, UK
[f] Lincoln Medical School, University of Lincoln, Brayford Pool Campus, Lincoln LN6 7TS, United Kingdom
[g] Institute for Biological and Medical Engineering, Schools of Engineering, Medicine and Biological Sciences, Pontificia Universidad Católica de Chile, Santiago, Chile

ARTICLE INFO

Keywords:
Cancer
PCSK9
Targeted drug delivery system
Liposome
Low-density lipoprotein receptor
Nanomedicine

ABSTRACT

Ligand-based targeting of the receptors that are overexpressed explicitly on cancer cells represents an effective drug delivery approach to enhance the chemotherapeutic efficacy. Proprotein convertase subtilisin/kexin type 9 (PCSK9) which is a serine protease enzyme primarily produced by the liver cells, can potentially be used as a targeting ligand. PCSK9 binds to the LDL-r on hepatocytes' surface, leading to endocytosis and endosomal degradation. High LDL-r expression, which is believed to meet the higher demand of the cholesterol and phospholipids to build proliferating cancer cell membrane, ensures selective uptake of the PCSK9 conjugated liposomes. In the present work, the PCSK9 conjugated liposomal system was developed to deliver paclitaxel (PTX) to cancer cells. The protein was conjugated by EDC and NHS in a two-step coupling reaction to the liposomes containing COOH-PEG_{2000}-COOH lipid. Conjugation was confirmed by NMR, and liposomes were further characterized by SEM and zeta sizer. PCSK9-conjugated liposomes showed high encapsulation efficiency of 69.1% with a diameter of *90.0* ± 4.9 nm. Long-term stability (30 days) study (Zeta potential: −9.88) confirmed excellent constancy and significant drug retention (58.2%). Invitro cytotoxicity and targeting efficiency was explored using MTS assay in human embryonic kidney cells (HEK293), liver hepatocellular cells (HEPG2), and a human colon cancer cell line (HCT116) for 24 h. PCSK9 conjugated liposomes exhibited significantly higher growth inhibition than the unconjugated (control) liposomes in HCT116 cell line ($p < 0.001$). The novel PCSK9 conjugated liposomes presented potent and precise in vitro anticancer activity and, therefore, are suggested for the first time as a promising targeted delivery system for cancer treatment.

1. Introduction

The narrow therapeutic index, severe side effects, and unfavorable pharmaceutical characters of many anticancer drugs, including doxorubicin, vincristine, cyclophosphamide, and paclitaxel (PTX), often restrict their long term clinical use [1–4]. To prevent non-specific targeting, side effects, and better patient compliance, these drugs are often administered in suboptimal dosages. Targeted delivery of anticancer drugs to the cancer cells and into the tumor microenvironment is seen as the potential remedy to this problem [5]. One of the primary objectives

* Corresponding authors at: Departamento de Química Orgánica, Facultad de Química y de Farmacia, Pontificia Universidad Católica de Chile, Av. Vicuña Mackenna 4860, 7820436, Macul, Santiago, Chile.
** Corresponding author at: SAAD Centre for Pharmacy and Diabetes, School of Pharmacy and Pharmaceutical Science, Ulster University, Coleraine, County Londonderry, Northern Ireland BT52 1SA, UK.
E-mail addresses: Nitinunimi@gmail.com (N.B. Charbe), m.tambuwala@ulster.ac.uk (M. Tambuwala), fzacconi@uc.cl (F.C. Zacconi).

https://doi.org/10.1016/j.biopha.2022.113428
Received 8 April 2022; Received in revised form 27 June 2022; Accepted 14 July 2022
Available online 15 July 2022

of the targeted drug delivery system is to increase the drug concentration in cancer cells and simultaneously limit its concentration in healthy cells. This is seen as the primary approach to diminish drug-related side effects. Nanotechnology-based systems like liposomes, micelles, linear polymers, branched polymers, and dendrimers hold tremendous potential to cargo the drugs to the desired site. Nano-systems composed of different lipids and polymers with different physicochemical and pharmacological properties have been comprehensively studied for drug and gene-based product delivery [6]. Simultaneously, the study of nanoparticles' interaction with a biological system, metabolic products of nanodrug delivery system, surface modification for cell-specific drug delivery, drug entrapment and release properties, simultaneous administration of more than one drug, and stability of nanoparticle and entrapped drugs is also underway [7–10]. Several anticancer drugs like PTX, doxorubicin, among others, have been successfully encapsulated in the nanoparticles [11–20]. Reports of the nanoparticles modified with the proteins and antibody (ligand) to target the pathologically induced proteins (e.g., receptors) on the cancer cells are also available [21,22]. Nanoparticles conjugated with the targeting ligands particular to the overexpressed surface proteins (e.g. surface receptors) on tumor cell surface represent an effective strategy [23–25]. Such approaches ensure the transport of anticancer drugs to the cancer cells and avoid a non-specific deposition.

Receptor-mediated endocytosis has been utilized as an attractive approach in cell surface targeting as it facilitates internalization and accumulation of therapeutic macromolecules at the site of action [26,27]. For such strategies to be clinically useful, appropriate cell surface receptors must be identified that are overexpressed, thus enabling more selective therapy with reduced side effects. Different plasma membrane receptors have received broad interest in the drug delivery community as a door for targeted nanoparticles. This may be due to their tissue-specific location or high expression in disease states such as cancer. To achieve the precession in drug delivery, linking of the ligand to the cargo, specific for the overexpressing receptors on the pathogenic cells is an attractive strategy [28–37].

In 2003, Seidah et al. identified the 9th member of the proprotein convertase family, proprotein convertase subtilisin/kexin type 9 (PCSK9) [38–40]. PCSK9 as a secreted protein is shown to bind to the LDL-r, and both are subsequently internalized by the endolysosomal pathway. Additionally, the binding of PCSK9 to LDL-r induces a conformational LDL-r switch such that it is normal recycling back to the plasma membrane is inhibited. Instead, the protein is delivered to lysosomes and degraded [40]. Although the liver is the primary LDL-r expression site; several studies have shown increased LDL-R expression in neoplastic cell lines. LDL receptor endocytic pathway can be used for the endocytosis based delivery of anticancer drugs to the hepatocytes and different types of cancer. Increased LDL-r expression is believed to meet the increased requirement of the fats and lipids to build a new double-layer cell membrane of the continuously proliferating cancer cells [41]. LDL-r was found to be upregulated in the mice model of colon cancer linked to the adiponectin difficency [42]. Furthermore, tumor necrosis factor was linked to the induction of the LDL-R on Hep G2 cells. These cells were also found to have stimulated hepatic synthesis of fat and its secretion in vivo [43]. TNF's role in inflammation-associated carcinogenesis has been studied widely and is one of the critical therapeutic targets [43]. Some prominent examples of the higher expression of LDL-r in disease state are: (1) Significant upregulation of the LDL-r in cancerous colonic mucosa has also been observed when compared with healthy tissue [44]; (2) Epidermoid cervical cancer cells, which starts in squamous cells were found to required 15 times more LDL than normal adrenal tissue and 50 times more than the non-cancerous gynecologic tissue [45]; (3) Endometrial adenocarcinoma which begins at the inner surface of the uterus was found to required 1 O times more LDL when compared with normal tissue [45]; Epidermoid cervical also called as squamous cancer and different gynecologic cancers have higher lipid requirement, and uptake than the normal tissues [46]; (4) Salivary gland cancer and stomach cancer were reported to have enhanced LDL uptake as compared to the normal cells [47]. Tumor cells of the central nervous system bind three times more to the LDL particles than non-cancerous brain cells, especially cancer of cerebellum, cancer of oligodendrocytes (oligodendroglioma), and meningioma [48]. (5) LDL uptake of the lung tumor cells was reported to have three times more uptake of the lipids then the adjacent noncancerous lung cells [49]; Cancer of fibroblast reported to uptakes high amount of LDL than normal tissue [50]; and High LDL receptor expression in breast cancer was found to be inversely correlated with the survival time [51,52]. This high LDL-r expression on cancer cells is believed to be a function of their increased demand for cholesterol and phospholipids to build new membranes for cell proliferation and division. Thus, targeting LDL-r for delivering cytotoxics and downregulating its expression is an attractive therapeutic strategy for several cancers.

In literature, various PTX loaded nanocarriers like emulsions, hydrogels, micelles, and liposomes are reported to reduce the associated side effects. This same system is also under observation to minimize the side effect of vehicle Cremophor EL used in Taxol formulation [53,54]. Allergic reaction associated with Cremophor EL has boosted to find the alternative vehicle to deliver the PTX [55,56]. Among these, albumin-bound PTX nanoparticles (nab-PTX) were approved for clinical use by FDA [57]. Nab-PTX, when compared with the Taxol, was found to be more efficient and less toxic. The patient's receiving nab-PTX was found to have less severe neutropenia episodes, hypotension, and bradycardia compared with Taxol. However, the irregularities in ECG were not rectified with nab-PTX [58]. Furthermore, the myocardial infarction is still the major adverse event observed in the patients administered with the nab-PTX. Therefore, the Cremophor EL free PTX delivery vehicle with less toxicity is required immediately to satisfy the urgent clinical need.

The liposomal formulation has already proven advantageous as compared to the other delivery systems in delivering water-insoluble drugs, better biocompatibility, stability, and ease of manufacturing [59–62]. In the present investigation, we developed a novel liposomal PTX formulation in PEGylated liposome conjugated with PCSK9. Here, the LDL-targeting properties of PCSK9 were merged with the drug carriage properties of liposomes. This approach also simultaneously reduces the quantity of the LDL-r, which the cancer cells utilize to uptake the lipids and support the synthesis of the new cell membrane, an important hallmark of cancer. Therefore, the proposed approach offers the dual benefit of localized delivery for the treatment of hepatocellular and other LDL-R expressing carcinoma and reduction of the critical receptor principally used by the cells for proliferation. This approach will help to address the encapsulation of poorly soluble and acid-labile drugs, thus permitting them to achieve their anticipated therapeutic action. Targeting cancer here will be via PCSK9, but additional enrichment will be obtained by the enriched permeation and retention effect.

2. Material and methods

2.1. Materials

Soybean lecithin (SPC) and Cholesterol was obtained from AK Scientific, USA, 1,2–distearoyl-*sn*-glycero-3-phosphocholine (DSPC), 1,2–distearoyl-*sn*-glycero-3-phosphoethanolamine-N-[carboxy(polyethylene glycol)− 2000]sodium salt (DSPE-PEG(2000)Carboxylic acid) and PTX (PTX) were procured from Sigma Aldrich (Ludwigshafen, Germany). MTS (Promega) was obtained from Sigma-Aldrich (Merck KGaA, Darmstadt, Germany). Roswell Park Memorial Institute (RPMI)-1640 medium (31800–022), Dulbecco's modified Eagle's medium (DMEM; 12100–061), DMEM/Nutrient Mixture F-12 (DMEM/F12; 12400–024), fetal bovine serum (FBS; 10437028), penicillin-streptomycin solution (P/S; 15140–122) and 2.5% (w/v) trypsin solution (15090–046) were bought from Gibco (Thermo Fisher Scientific, Inc.).

Table 1
LC/MS&MS Gradient Condition for Elution of PTX.

Sr. No	Time (min)	Flow (ml/min)	Mobile Phase A (%)	Mobile Phase B (%)
1	0.00	0.50	50	50
2	1.00	0.50	50	50
3	2.00	0.50	0	100
4	5.50	0.50	0	100
5	6.00	0.50	50	50
6	700	0.50	50	50

2.2. PTX-loaded liposomes (CTR S1-S6)

PTX-loaded liposomes were formulated by the previously reported thin-film hydration method. [27,28] Briefly, SPC, cholesterol, DSPC, DSPE-PEG(2000) carboxylic acid, and PTX were dissolved in chloroform (Sigma-Aldrich) at a molar ratio of 95:2:1:2 in a round-bottom flask. The organic solvent from the mixture was then removed at 40 °C by using a rotary evaporator leading to the formation of lipid film on the inner surface of the round bottom flask. The lipid film thus formed was then hydrated with the water at 45°C. The multilaminar lipid suspension was downsized to homogeneous unilamellar liposomes using ultrasonication and an Avanti's Extruder (SKU: 61000–1Ea) with 0.1 μm pore size polycarbonate filter. Unilaminar liposomes thus obtained were used as the control and to conjugate the PCSK9 protein. Free PTX was separated from the PSCK9 conjugated liposomes by size separation column made up of Sephadex G100. To evaluate the concentration and encapsulation efficiency, the encapsulated drug was extracted using 1% Trixton, diluted with methanol, and 10 μl of the diluted extraction was injected into SCIEX Triple QuadTM 4500 + - QTRAP® LC-MS/MS system. Reverse phase chromatographic separation was achieved on Inertsil C8–3, 100 mm × 4.6 mm× 3 μm of GL Science (Japan) Column, which was maintained at 40 ° C. The separation was performed using a gradient elution of ACN 0.1% formic acid: H_2O 0.1% formic acid from 50:50–00:100 (v/v) within 4 min at a flow rate of 0.5 ml/min. The injection volume of the unknown PTX sample was 10 μl.

2.3. Preparation of PTX-loaded PCSK9 conjugated liposomes (Sample 1–6)

PCSK9 was conjugated with the COOH-PEG_{2000}-COOH containing liposomes in a two-step conjugation reaction. In short, the COOH group of the lipid was activated by incubating the liposomes with EDC and NHS for 30 min with moderate stirring. The reaction mixture was then neutralised with 0.01% solution of sodium hydroxide. The NH_2 group of the PCSK9 protein was then linked with the activated COOH group (NHS) of the liposomes. The conjugation reaction was carried out for 24 h at 4 °C.

Unreacted PCSK9 and activating reagents were removed by size exclusion chromatography. The PTX entrapped in the lipid nanoparticles was quantified by LC-MS/MS assay. To evaluate the EE of the conjugated and unconjugated liposomes, the encapsulated drug was extracted using 1% Trixton 100 and diluted with acetonitrile. 10 μl of the aliquot was analyzed using LC-MS/MS. The EE (%) of PTX in CTR-PTX-LIP and PCSK9-PTX-LIP was calculated by populating the observed values in the following equation:

$EE\ (\%) = W_{encapsulated}/W_{total} \times 100\%$.

Where EE= encapsulation efficiency, W_{total}= total amount of PTX in the lipid nanoparticles, $W_{encapsulated}$ = amount of PTX encapsulated.

2.4. PTX quantification

The highly sensitive tandem combination of LC and MS was used to plot the calibration curve for PTX. Calibration curve plotting and other analysis were done using Analyst 1.6.2 software. PTX was separated using GLSciencies, Inertsil C8–3, 100 mm × 4.6 mm× 3 μm column. The analyte was eluted with a gradient elution started from 50%− 50% of Mobile phase A (water + 0.1% formic acid) and Mobile Phase B (acetonitrile + 0.1% formic acid). The flow rate was maintained at 10 μl per minute, and the column temperature was maintained at 40 °C. Details of the gradient of the mobile phase is given in Table 1. Mass analysis was conducted by a Triple Quad 4500 Quantum MS/MS system equipped with an electrospray ionization interface operated in the positive ionization mode. PTX quantification was accomplished in multiple reaction monitoring (MRM) by monitoring the transition of *m/z* 854.301 → 286.000 and *m/z* 854.301→ 509.100. In short, a 25 μl aliquot of liposomes (CTR-PTX-LIP and PCSK9-PTX-LIP) was taken in the Eppendorf tube and mixed with the 25 μl of 1% Trixton. After gentle shaking for 2 min, the volume was makeup to 1000 μl with CH_3OH. 10 μl of the diluted sample, filtered with 0.1 μm syringe filter was injected onto the column (Inertsil C8–3, 100 mm × 4.6 mm×3 μm of GL Science, Japan), which was maintained at 40 ° C. Concentration of the PTX in liposome was then calculated from the linear calibration cure constructed in the range of 10–100 ppm.

2.5. Characterization of liposomes

The mean size and zeta potential of lipid nanoparticles were analysed by dynamic light scattering (Malvern Zetasizer Nano ZS; Malvern Instruments Ltd., Malvern, UK). All the experiments were conducted in triplicate. The physical characterisation of the liposomes was investigated after 10 times dilution with filtered deionized water. The proton NMR spectra confirmed PCSK9 conjugation with the liposome. For proton NMR spectra, PCSK9-PTX-LIP and CTR-PTX-LIP were freeze-dried for two days. The freeze-dried product was then dissolved in the deuterated chloroform, and NMR was recorded on Brucker Advance III HD 400 NMR spectrometer (400 MHz). The SEM/TEM images were acquired using Quanta 250 FEG scanning electron microscopes equipped with a high-resolution digital camera to observe structural features.

2.6. In vitro release study

In vitro release of PTX from the PCSK9-PTX-LIP and CTR-PTX-LIP was investigated using the dialysis method. PBS (pH 7.4) was used as a release medium. Liposomes separated from the untrapped PTX was diluted with release medium PBS (pH 7.4). The dilution volume was tuned to get the final drug concentration of 100 μg/ml. A tube of the molecular weight cut-off of 12000 was selected for the dialysis. Dialysis tubes containing diluted liposomal formulation were placed into the falcon tube containing 10 ml of PBS (pH 7.4). The dialysis of PTX was carried out by incubating the falcon tubes at 37 °C with constant stirring. The release medium was collected and replaced with the fresh medium at the scheduled time intervals (0.5, 1,2,4,8,12,24 h). The PTX released in the medium was quantified by LC-MS/MS assay method described above.

2.7. Stability

Stability of control (CTR-PTX-LIP) and PCSK9 conjugated liposomes (PCSK9-PTX-LIP) was estimated by detecting the change in particle size, zeta potential, PDI, and the unreleased PTX during storage. LC-MS/MS assay method described above was used to quantify the retained PTX in nanoparticles.

2.8. Cell culture

Human embryonic kidney cells (HEK293), liver hepatocellular cells (HEPG2), and a human colon cancer cell line (HCT116) were acquired from the American Type Culture Collection (ATCC; Manassas, VA, USA). HEK293 and HEPG2 cells were developed in DMEM/F12 medium complemented with 10% and 5% FBS, respectively. On the other hand, HCT116 cells were selected to grow in RPMI-1640 medium

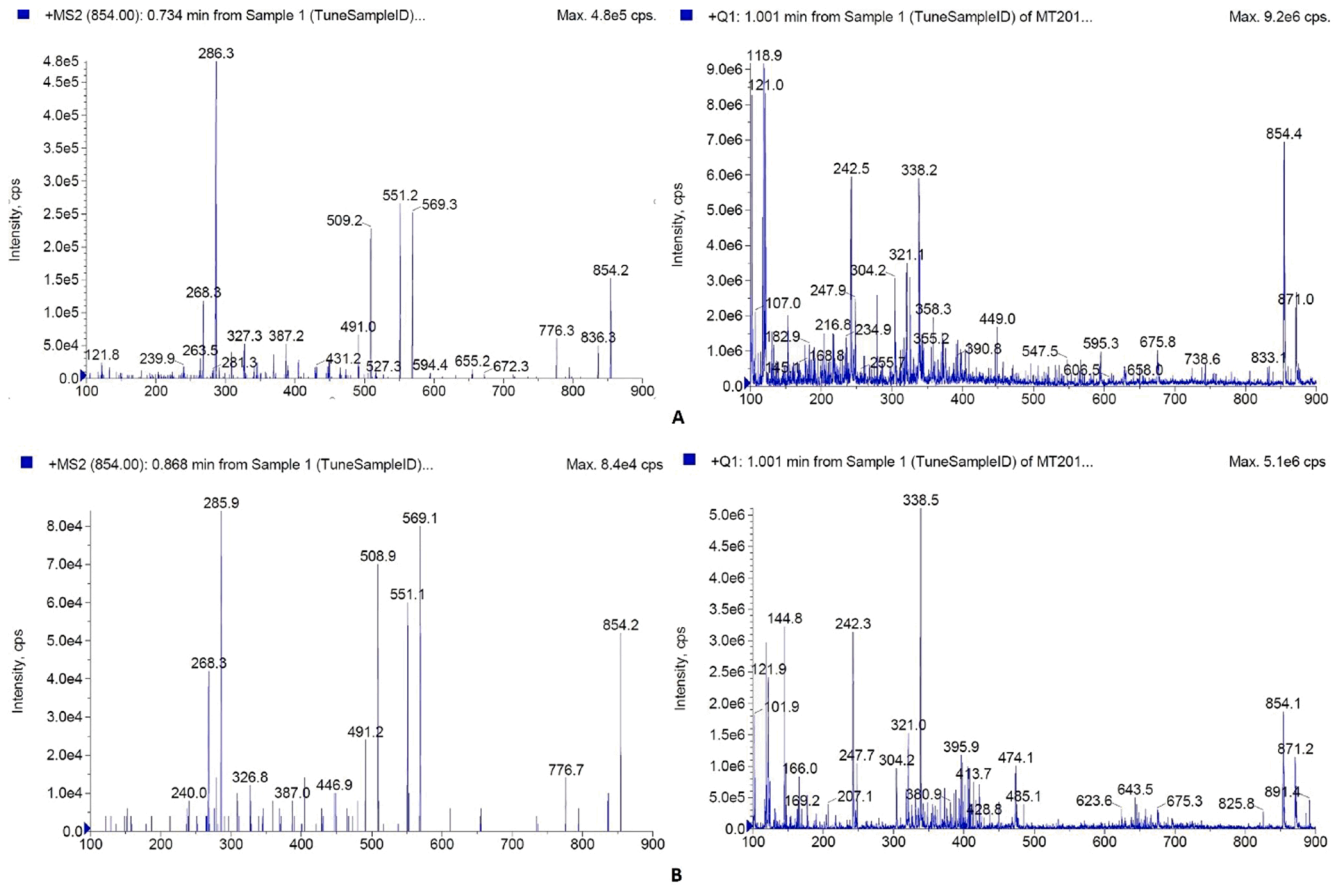

Fig. 1. a PTX Fragmentation in Methanol, b:PTX fragmentation in Acetonitrile.

complemented with 10% FBS. All cultures were maintained in the appropriate medium containing 100 U/ml P/S and were incubated in an atmosphere comprising of 5% CO_2 at 37 °C.

2.9. In vitro cellular cytotoxicity

For cell viability study, the CellTiter 96® AQ_{ueous} One Solution Reagent containing novel tetrazolium compound inner salt; MTS(a)] and an electron coupling reagent (phenazine ethosulfate) was used. During the assay, tetrazolium is enzymatically reduced by proliferating cells into formazan, which is a soluble color compound. The magnitude of insoluble formazan in the tissue culture medium indicates the degree of cellular activity. Assays were carried out by adding a constant amount of the MTS reagent directly to wells and then incubated for the appropriate time. After incubation, the change in the color due to the formation of formazan was analyzed by reading the culture plate at 490 nm. The amount of the formazan produced is relative to the total number of metabolizing cells. Overall, culture plates (96 well) containing 5×10^3 cells/well were incubated with the appropriate growth medium containing FBS at 37 °C. Proliferating cells were then treated with two-fold serially diluted control (CTR-PTX-LIP/PTX loaded liposomes), sample (PCSK9-PTX-LIP/PTX loaded liposomes) at a concentration ranging from 0.195 and 50 nM for a total 24 h. After being washed with PBS twice, cells were incubated at 37 °C with the 0.5 mg/ml MTS prepared in serum-free medium for 4 h. Subsequently, the growth medium was removed from the well, and purple formazan crystals formed due to the enzymatic reaction within the cells were dissolved in dimethyl sulfoxide. Light absorbed in the visible range was measured at 540 nm using Biotek plate reader.

3. Results and discussion

3.1. LC-MS/MS estimation of PTX

For the preparation of the calibration curve, 1 mg/ml PTX solution in methanol and acetonitrile was made separately and injected directly into the mass spectrophotometer (Fig. 1a & b). The fragmentation and signal intensity of both the solutions was compared. Due to the better signal of the PTX in methanol (Fig. 1), PTX in methanol was used for further analysis. Parent peak at m/Z 854.1 was found to be consistent with the molecular formula $C_{47}H_{51}NO_{14}$. Electrospray ionization mass spectral fragmentation at *m/z* at 776.3, 569.3, 551.2 and 509.2 confirms the presence of the PTX skeleton. [63] The mother solution of PTX was diluted to get a stock solution of the concentration of 0.01 mg/ml stock. The stock solution was then used to construct the linear calibration curve with 6 points within the range of 0.1–1.0 ppm. PTX standard calibrators gave a linear curve over the dynamic range of 0.1–1.0 ppm with an r^2 coefficient of 0.9992. Precision and accuracy were studied by 3 replicates of quality controls (Low, Medium and High). Both the mother and stock solution were kept at − 80 °C for further use. Mother solution was stable over a period of one year.

3.2. Determination of optimal concentration of lipids for maximum PTX entrapment

Lipids and PTX (SP:CHOL:DSPC:DSP-PEG-2000-COOH: PTX) mixture was used in a various molar ratio to determine the maximum PTX encapsulation ratio and lowest particle size (**Error! Reference source not found.**). The concentrations of SP:CHOL:DSPC:DSP-PEG-2000-COOH:PTX were varied from 80:20:00:00:01–75:15:05:05:01 molar ratio. Results revealed that the encapsulation ratio was increased

Table 2
Effect of Lipid concentration on PTX entrapment ratio and liposome size.

Molar ratio of lipid (SP:CHOL: DSPC:DSP-PEG-2000-COOH: PTX)	Liposomal Size (nm)		Encapsulation ratio	
	CTR-PTX-LIP	PCSK9-PTX-LIP	CTR-PTX-LIP	PCSK9-PTX-LIP
80:20:00:00:01	134.0 ± 7.8	140.0 ± 9.1	48	31
85:15:00:00:01	154.0 ± 9.3	168.0 ± 10.8	57	38
90:10:00:00:01	161.0 ± 9.4	177.0 ± 7.9	39	30
75:20:05:00:01	139.0 ± 10.8	151.0 ± 10.1	58	51
80:15:05:00:01	124.0 ± 8.3	152.0 ± 10.7	64	59
85:10:05:00:01	124.0 ± 5.1	177.0 ± 8.4	44	47
70:20:05:05:01	109.0 ± 4.8	115.0 ± 4.8	75	71
75:15:05:05:01	90.0 ± 4.9	126.0 ± 6.1	76	70
80:10:05:05:01	111.0 ± 8.7	130.0 ± 10.2	69	64

Mean ± S.D. (= 3). < 0.05 between molar ratio of different lipids.

Table 3
Particle size, polydispersity index, zeta potential and encapsulation efficiency.

Liposomes	Particle Size (nm) (mean ±SD*)	Polydispersity Index (PDI) (mean±SD*)	Zeta Potential (mV)	Encapsulation efficiency (%)
CTR-PTX-LIP	90.0 ± 4.9	0.046 ± 0.003	-9.31	69.1
PCSK9-PTX-LIP	126.0 ± 6.1	0.136 ± 0.004	-2.89	64.5

N = 3*; Values represent the mean±SD.

with the addition of 0.5 molar ratio of DSPC with the simultaneous reduction of the molar ratio of SP from 90 to 70 molar ratio. Simultaneously, the liposomal size was found to decrease with the addition of DSPC in the formulation. For the preparation of CTR-PTX-LIP and PCSK9-PTX-LIP liposomes, a molar ratio of 75:15:05:05:01 (SP:CHOL: DSPC:DSP-PEG-2000-COOH: PTX) was finalized. CHOL molar ratio was found to have no remarkable effect on the encapsulation ratio and particle size. The liposomal size of the final formulation obtained was 90 ± 4.9 nm and 126 ± 6.1, and EE was 76% and 70% for CTR-PTX-LIP and PCSK9-PTX-LIP, respectively (Table. 2).

3.3. Zeta potential of CTR-PTX-LIP and PCSK9-PTX-LIP liposomes

The zeta potential value is a vital physical parameter that can affect the stability of the lipid nanoparticles and overall drug circulation time in vivo. The zeta potential was found to be − 9.31 and − 2.89 mV for CTR-PTX-LIP and PCSK9-PTX-LIP, respectively. Due to the favorable zeta potential, it is expected that the prepared liposomes will not only have a sustained anticancer activity, but it will be more specific towards the cancer cells due to PCSK9 mediated endocytosis. Simultaneously, less accumulation of anticancer drugs in healthy tissues was expected, thereby limiting its off-site toxicity. Table 3 summarized the mean particle size and polydispersity index (PDI) of the PCSK9 conjugated and unconjugated lipid nanoparticles.

The size of the PCSK9 conjugated liposomes was found to be 126.0 ± 6.1, whereas the particle size of the non-targeted liposomes (Control liposomes) was found to be 90.0 ± 4.9 nm. Increases in the particle size of the PCSK9 conjugated liposomes may be attributed to the additional protein molecules linked to it. The PDI of control (PTX loaded, PCSK9 unconjugated) and sample (PSCK9 conjugated) have shown a very narrow size distribution (***CTR-PTX-LIP***: 0.046 & ***PCSK9-PTX-LIP***: 0.136), indicating the uniformity of the size (Table 3). The higher negative zeta potential value of control liposomes as compared to the PCSK9-PTX-LIP indicates a reduction in the positive charge because of charge neutralization when conjugated with positively charged PCSK9 protein. At pH below its isoelectric point (PI), protein carries a net positive charge, and above PI protein carries a negative charge. The prepared conjugated liposomes were suspended in a neutral medium. PI value of the PCSK9 is 6.1, which is well above its PI values. The higher pH of the suspended medium, then the actual PI values of PCSK9 explain the net positive and lower net negative charge of the PCSK9 conjugated liposomes.

3.4. Confirmation of PCSK9 conjugation with 1 H NMR spectrophotometer

According to the ^{1}H NMR spectra of PCSK9 conjugated liposomes, a characteristic peak at 6.54 ppm was observed belongs to the amide hydrogen (N-H) part of the newly formed amide linkage (Fig. 2a). Such amide proton peak was not found in CTR-PTX-LIP (Fig. 2b). In ^{1}H NMR spectra of PCSK9 conjugated liposomes, the triplet at 1.11 confirmed the –CH2 protons of the amino acids PCSK9. Furthermore, singlet at 4.38 ppm confirms the conjugation between the free -NH_2 group of

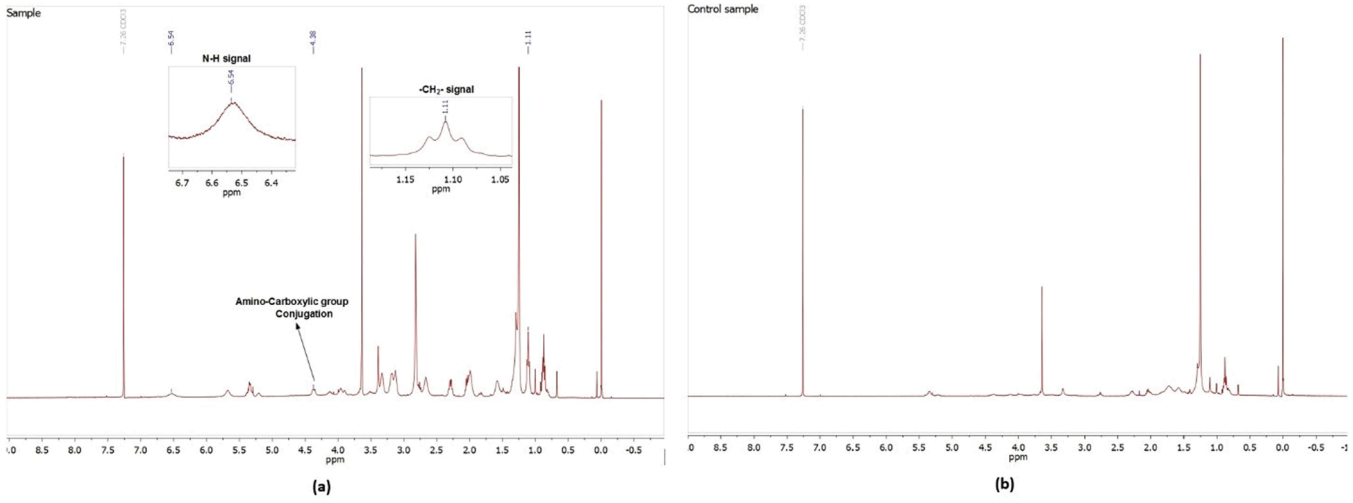

Fig. 2. H1 NMR of (a) PCSK9-PTX-LIP(Sample) and (b) CTR-PTX-LIP (b) (Control).

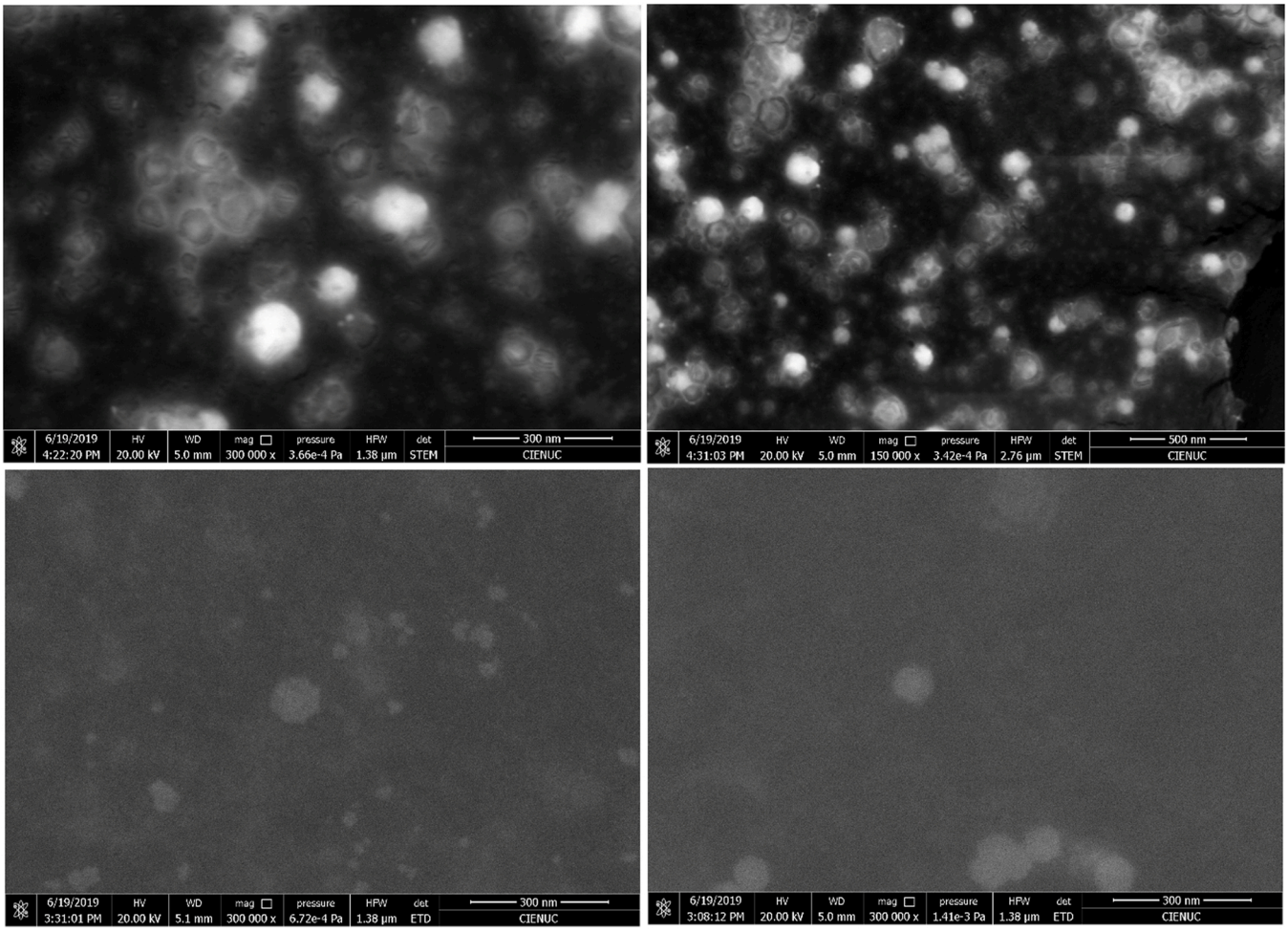

Fig. 3. Transmission electron microscope (TEM) image of (A) Non-targeted liposomes (CTR-PTX-LIP) in 100 nm scale and (B) Targeted liposomes (PCSK9-PTX-LIP).

Table 4
Stability test of liposomes.

Liposome	Lipid Molar Ratio	Mean Particle Size		Zeta Potential		Encapsulation efficiency (%)	
		Initial	After 30 days	Initial	After 30 days	Initial	After 30 days
CTR-PTX-LIP	*75:15:05:05:01*	90.0 ± 4.9	101.0 ± 3.5	-10.69	-15.5	69.1 ± 3.9	62.3 ± 4.6
PCSK9- PTX-LIP	*75:15:05:05:01*	126.0 ± 6.1	139.0 ± 5.6	-5.76	-9.88	64.5 ± 4.7	58.2 ± 5.2

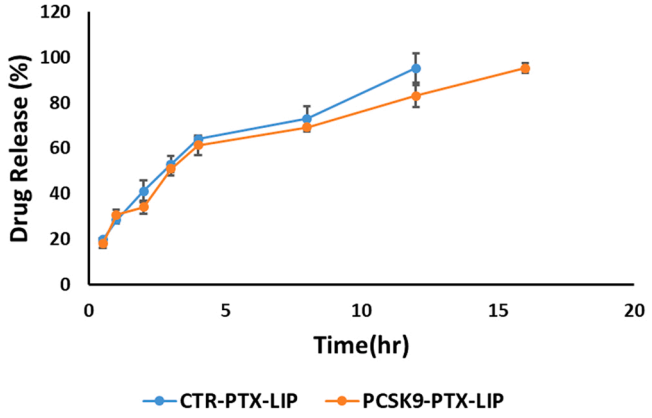

Fig. 4. In-vitro drug release study of non-targeted and targeted liposomes in phosphate-buffered saline (pH 7.4).

PCSK9 and the -COOH group of control liposomes [64].

3.5. Morphological characterization of CTR-PTX-LIP and PCSK9-PYX-LIP liposomes

In the SEM/TEM observation (Fig. 3), the PEGylated and PCSK9-PEGylated liposomes containing PTX prepared were about 130 nm in size and had a comparatively circular smooth surface. These results are in agreement with DLS analyzer measurements. The present result confirms the particle size and morphology. This further confirms the suitability of the method used for the conjugation of the PCSK9 protein to the liposome.

3.6. Stability test of liposomes at storage condition

As summarized in Table 4, the particle size and EE of both PCSK9 conjugated and unconjugated liposomes suspended in PBS solution (pH 7.4) were almost unchanged during storage (30 days). During storage

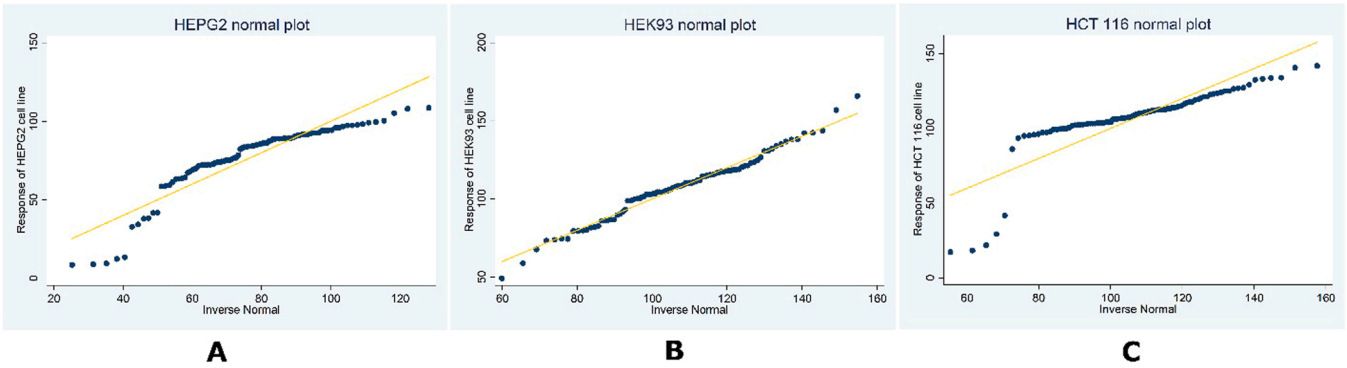

Fig. 5. The Shapiro-Wilk test is used to check if the response of drugs & time on HEPG2, HEK93, HCT116 cell lines are normally distributed. Since the p-value $= 0.000 < 0.05$, there is statistical reason to reject H_0 and conclude that the data is not normally distributed for HEPG2 and HCT116 cell lines, whereas for the HEK93 cell lines the p-value $= 0.39509 > 0.05$, there is no statistical reason to reject H_0 and conclude that the data is normally distributed.

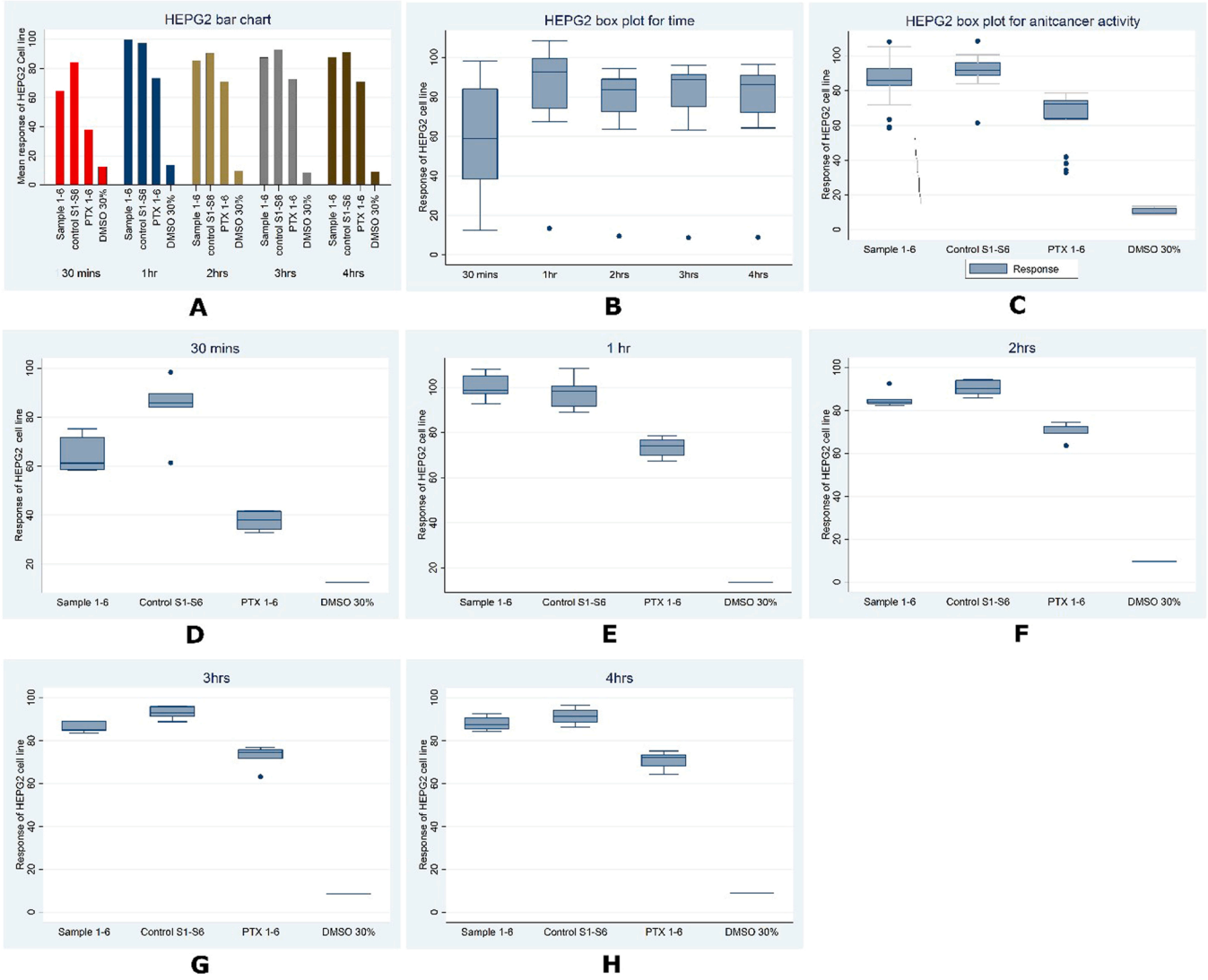

Fig. 6. Comparison of the effect of PTX loaded PCSK9-conjugated liposomes(Sample 1–6/ PCSK9- PTX-LIP), PTX loaded PCSK9-unconjugated liposomes (Control S1-S6/CTR-PTX-LIP), free PTX (1−6) and DMSO 30% effects on the HEPG2 cell line over the period (30 min, 1,2, 3, and 4 h) (A) Mean response of HEPG2 cell line against the PXT loaded PCSK9 conjugated, Unconjugated liposomes, Free PTX and DMSO 30% (B) Box plot of the HEPG2 cell lines response towards all the formulations (C) Box plot of the anticancer activity of all the formulations and media, (D)(E)(F)(G)(H) Box plot of the HEPG2 cell line response at 30 min, 1, 2, 3, and 4 h respectively.

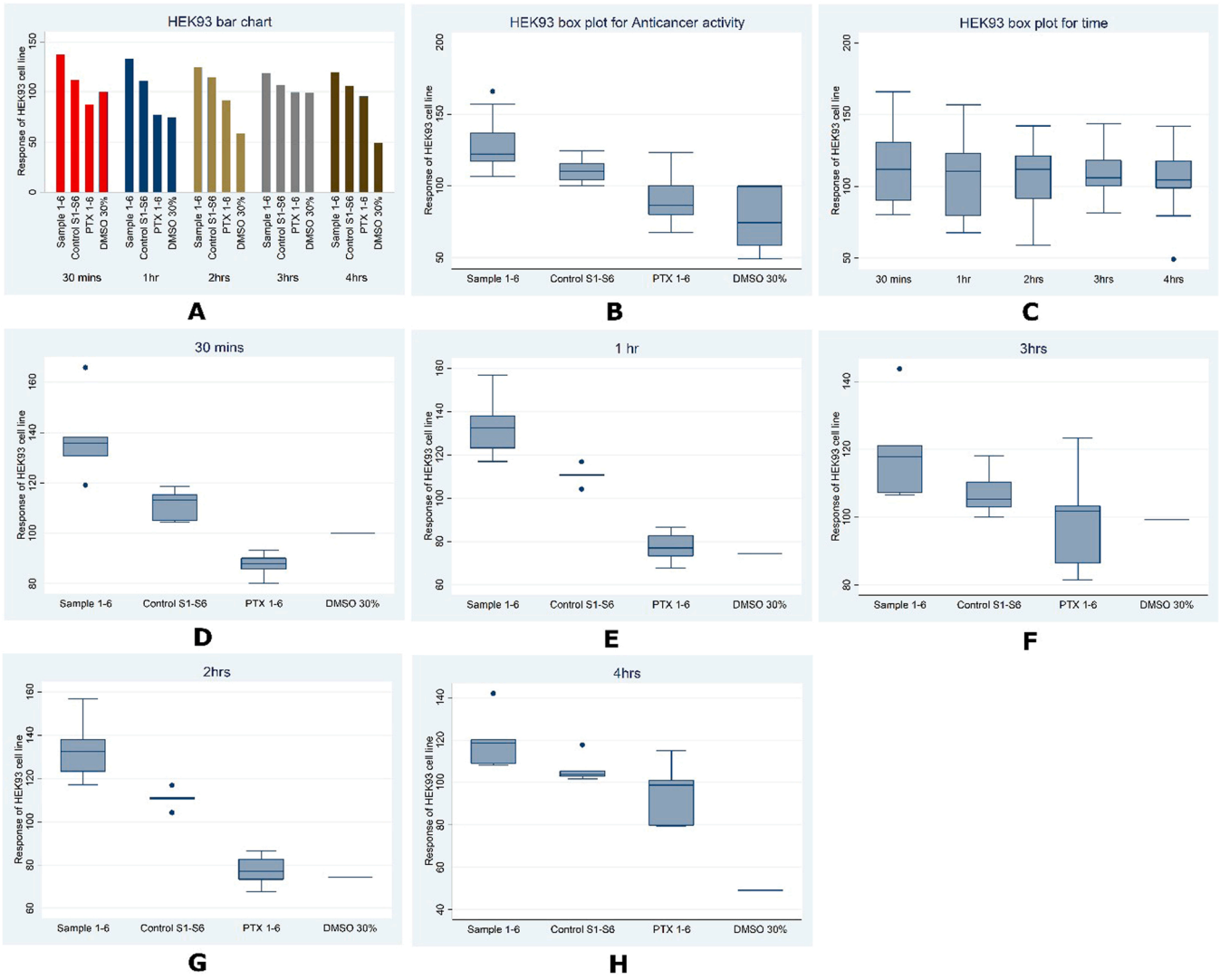

Fig. 7. Comparison of the effect of PTX loaded PCSK9-conjugated liposomes(Sample 1–6/ PCSK9- PTX-LIP), PTX loaded PCSK9-unconjugated liposomes (Control S1-S6/ CTR- PTX-LIP), free PTX (1−6) and DMSO 30% effects on the HEK93 cell line over the period (30 min, 1, 2, 3, and 4 h) (A) Mean response of HEK93 cell line against the PXT loaded PCSK9 conjugated, Unconjugated liposomes, Free PTX and DMSO 30% (B) Box plot of the HEK93 cell lines response towards all the formulations (C) Box plot of the anticancer activity of all the formulations and media, (D)(E)(F)(G)(H) Box plot of the HEK93 cell line response at 30 min, 1,2,3, and 4 h respectively.

time, the nanoparticles have exhibited excellent stability and drug retention. Overall the results confirmed that the PCSK9 conjugated and controlled liposomes stored for 30 days at 4 °C in PBS solutions (pH 7.4) were stable with no significant change in the Zeta potential, particle size, and drug encapsulation efficiency.

3.7. Drug encapsulation

The CTR-PTX-LIP and PCSK9-PTX-LIP were found to encapsulate 69.1% and 64.5% of PTX, respectively. As compared to the control, PCSK9 conjugated liposomes showed a minor decrease in drug encapsulation efficacy. This is attributed to the disturbance of the liposomal membrane during the conjugation of the PCSK9 protein to the liposomes (Table 4) [65].

3.8. In vitro release

Fig. 4 relates the cumulative release of PTX from control and PCSK9 conjugated liposomes in PBS (pH 7.4). The release of PTX from PCSK9 conjugated (Sample) and unconjugated liposomes containing PTX (Control) were found similar. The PTX release rate from the PCSK9 conjugated liposomes was found to be slow and sustained without any burst release. The % of PTX released from the unconjugated and PCSK9 conjugated lipid nanoparticles was found to be 96% and 91% after 12 and 36 h, respectively. No further increase in the drug concentration in buffer solution was observed after 48 h of dialysis. PCSK9 conjugated onto the liposome is thought to be the reason for the slower release rate of PTX when compared with unconjugated nanoparticles. The $t_{50\%}$ (time taken by the 50% of the drug to appear) of the formulations was about 1.2 and 3 h for control and PCSK9 conjugated liposomes, respectively. The average release of the PTX from the PCSK9 conjugated liposomes is relatively low compared to the unconjugated liposome; hence the former could also be used for sustained and controlled drug release in systematic circulation.

3.9. Anticancer assay

3.9.1. Cytotoxicity

The anticancer activity was carried out to determine the effect of PTX, liposomal PTX, and PTX loaded PCSK-9-liposome. PTX dissolved in

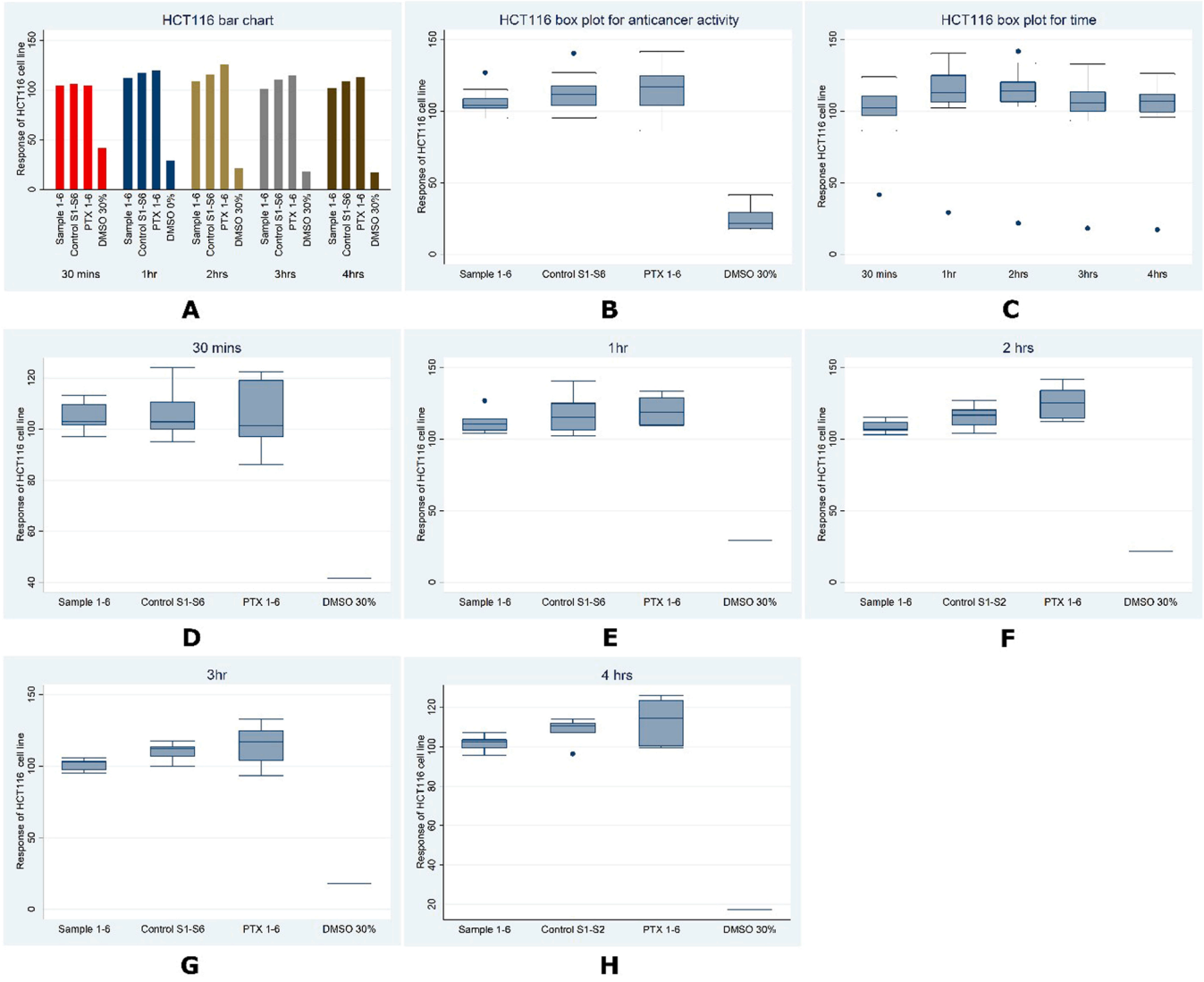

Fig. 8. Comparison of the effect of PTX loaded PCSK9-conjugated liposomes(Sample 1–6/ PCSK9- PTX-LIP), PTX loaded PCSK9-unconjugated liposomes (Control S1-S6/CTR- PTX-LIP), free PTX (1 −6) and DMSO 30% effects on the HCT116 cell line over the period (30 min, 1, 2, 3, and 4 h) (A) Mean response of HCT116 cell line against the PXT loaded PCSK9 conjugated, Unconjugated liposomes, Free PTX and DMSO 30% (B) Box plot of the HCT116 cell lines response towards all the formulations (C) Box plot of the anticancer activity of all the formulations and media, (D)(E)(F)(G)(H) Box plot of the HCT116 cell line response at 30 min, 1, 2, 3, and 4 h respectively.

DMSO was used as the control and the solvent vehicle (30% DMSO) was used as the negative control. The cytotoxic effect was observed for 30 min, 1, 2, 3, 4, 24 h on three cell lines plate (HEPG2, HEK93, HCT116). Tests were conducted at a 95% confidence level, and the decision rule was based on rejecting the null hypothesis if the p-value is less than 0.05.

3.9.2. *Experimental design and layout (Fig. 5)*

The experiment consisted of 3 cell lines plates (HEPG2, HEK93, and HCT116), which were treated with PTX, liposomal PTX, and PCSK conjugated liposome at six different concentrations. The cytotoxic effects were observed at five levels (separate plates for 30 min, 1 h, 2 h, 3 h, and 4 h), and all the plates were again observed to check the effect of the drug after 24 h (Fig. 5).

3.9.3. *MTS assay*

To assess the formulation effect, we compared the anticancer effect of liposomal PTX (CTR-PTX-LIP/Sample 1–6, PCSK9 conjugated Liposomes (PCSK9-PTX-LIP), free PTX (PTX 1–6), and DMSO 30%) on three different cancer cell lines, namely HEPG2, HEK293, and HCT116. The cytotoxic results are presented in Figs. 6–9. The cytotoxic effect of control (CTR-PTX-LIP) and PCSK9 conjugated liposomes (PCSK9-PTX-LIP) was found almost similar or better than the PTX treated cells.

When loaded into control (Control S1-S6/CTR-PTX-LIP) and PCSK9 conjugated liposomes (Sample 1–6/ PCSK9- PTX-LIP), PTX showed lesser toxicity in HEPG2 cells than the free drug. However, PCSK9 conjugated liposome at any given time (0.30, 1, 2, 3, and 4 h), and concentration was found slightly better than free drug (Fig. 9: A). The difference in the cytotoxic effect was more pronounced in the first half-hour after the treatment (Fig. 6. D). The same 96 well microplates, when observed after the 24 h, control, PCSK9 conjugated liposome, and free drug (PTX 1–6), almost have shown similar cytotoxic activity (Fig. 9: A). When HEK293 cell lines were treated similarly, free drugs were found marginally superior, then the liposomal PTX after 0.30, 1, 2, 3, 4, and 24 h (Fig. 7 & 9:B). When HCT116 cell was treated with control, sample, and free drug, PCSK9 conjugated liposomes were not only found superior then the unconjugated liposomes (control), but its cytotoxic activity was found better than the free drug (Fig. 8 & 9:C). The difference in the activity was statistically significant after 2 h of the treatment.

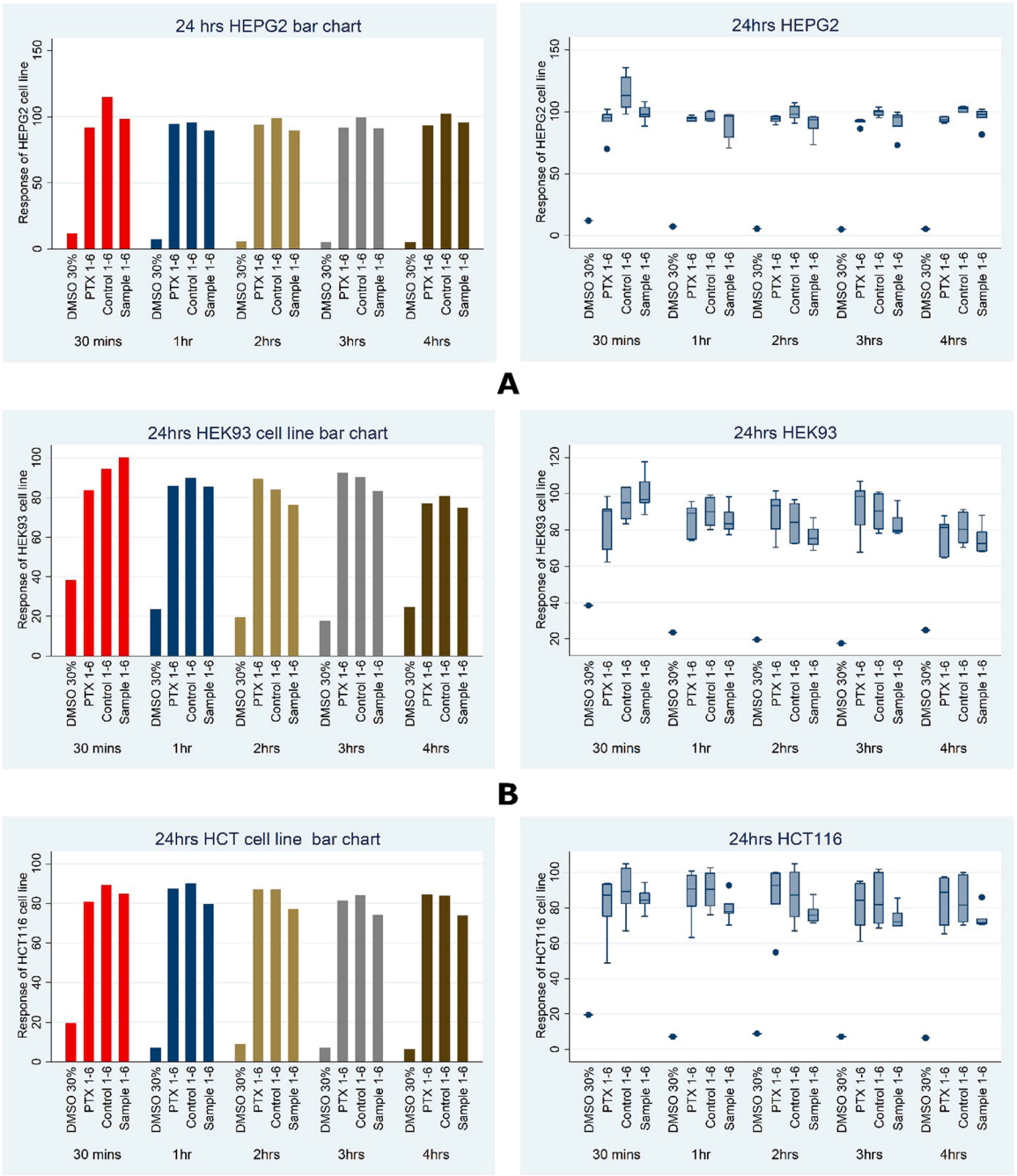

Fig. 9. Comparison of the effect of PTX loaded PCSK9-conjugated liposomes (Sample 1–6/PCSK9- PTX-LIP), PTX loaded PCSK9-unconjugated liposomes (Control 1–6/CTR- PTX-LIP), free PTX and DMSO 30% effects on the HEPG2, HCT116, and HEK93 cell after 24 h (A:HEPG2 Cell line, B:HEK93 Cell line, C:HCT116 Cell line).

3.9.4. Statistical analysis

The Kruskal-Wallis H test, also called one-way ANOVA, was used as the assumption of normality of the data set is not met. This test is used to determine if there are statistically significant differences between the response of formulations on cell lines. Table 5 shows a statistically significant difference in responses between the treatments on HEPG2, HEK93, and HCT116 cell lines. Since the N^2 (3)= 56.199, $p = 0.0001 < 0.05$, N^2 (3)= 64.766, $p = 0.0001 < 0.05$ and N^2 (3)= 24.934, $p = 0.0001 < 0.05$ for HEPG2, HEK93 and HCT116 respectively we rejected the null hypothesis of no significant difference. Kruskal-Wallis H test was also used to check the difference in response over the period of time. Table 6 shows that there is a statistically significant difference between the time observed (N^2 (4)= 1.698, $p = 0.002 < 0.05$) for HEPG2 cell line. For the HEK93 cell line, there is no statistically significant difference in responses between the time observed. As the N^2 (4)= 1.358, $p = 0.851 > 0.05$, we failed to reject the null hypothesis of no significant difference in the response over the period of time. For the HCT116 cell line, a statistically significant difference in response was observed over different time intervals. Since N^2 (4)= 15.060, $p = 0.005 < 0.05$, we failed to reject the null hypothesis of no significant difference.

Table 5
Non-parametric Test for formulation response (Kruskal-Wallis equality-of-populations rank test).

		Formulations	N	**Mean Rank**	**Chi-Square**	**p-value**
HEPG2	Response	*Sample 1–6	30	56.03	56.199 (3)	0.0001
		* *Control S1-S6	30	70.33		
		PTX 1–6	30	25.13		
		DMSO 30%	5	3.00		
		Total	95			
HEK93	Response	*Sample 1–6	30	76.03	64.766	0.000
		**Control S1-S6	30	51.10		
		PTX	30	22.75		
		DMSO 30%	5	12.70		
		Total	95			
HCT116	Response	*Sample 1–6	30	37.57	24.934	0.0001
		**Control S1-S6	30	53.47		
		PTX 1–6	30	60.47		
		DMSO 30%	5	3.00		
		Total	95			

* PCSK9- PTX-LIP, **CTR- PTX-LIP.

Table 6
Non-parametric Test for time observed (Kruskal-Wallis equality-of-populations rank test).

		Formulations	**N**	**Mean Rank**	**Chi-Square**	**p-value**
HEPG2	Response	30 min	19	71.88	1.698(4)	0.002
		1 h	19	56.25		
		2 h	19	41.40		
		3 h	19	33.15		
		4 h	19			
HEK93	Response	30 min	19	51.89	1.358(4)	0.851
		1 h	19	46.26		
		2 h	19	51.42		
		3 h	19	43.11		
		4 h	19			
HCT116	Response	30 min	19	34.05	15.060 (4)	0.005
		1 h	19	60.84		
		2 h	19	61.00		
		3 h	19	43.32		
		4 h	19	40.79		

4. Discussion

In the present investigation, optimized PCSK9 conjugated liposomal formulation was developed with PTX as a model drug. Due to the site-specific delivery of the PTX by the PCSK9 conjugated liposomes, fewer side effects compared to the free drug is expected. The CTR-PTX-LIP (90 nm) and PCSK9-PTX-LIP (126 nm) were prepared easily with a lipid film hydration method. The entrapment efficiency of unconjugated (CTR-PTX-LIP) and conjugated liposomes (PCSK9-PTX-LIP) was 69.1% and 64.5% at the optimal lipid and PTX molar ratio.

To obtain the desired size and drug entrapment, the various concentration of the lipids and PTX were analyzed. Factors like lipid concentration, lipid drug ratio, cholesterol lipid ratio, and polyethylene glycol chain length not only severely affect the particle size and drug encapsulation capacity of the liposomes, but these factors also contribute to the overall stability of the liposomes. The model anticancer drug, PTX, and the lipids used to prepare the liposome membrane are water-insoluble. In the present work, lipids like SP, CHOL, DSPC, DSP-PEG-2000-COOH, which are amphiphilic fatty acids are used. A thin layer of the lipids formed after evaporation of the chloroform was hydrated with water. As the PTX is lipid-soluble, PTX gets entrapped inside the lipid layer of the newly formed vesicles. The outer layer of the liposome is hydrophilic, allowing suspension in an aqueous solution. The bulky PEG head with highly hydrated groups on the liposome surface serves to sterically inhibit hydrophobic and electrostatic contacts with immune proteins, which helps in the decrease recognition by the mononuclear phagocyte system. PTX, which is captured in the lipid layer of the liposome, does not come into contact with the aqueous solution.

Various batches of the liposomes composed of monounsaturated lipid (PC), Saturated lipid (DSPC), Polyunsaturated lipids (SPC) PEG linked saturated lipids with COOH functional groups and cholesterol were analysed for their size and drug entrapment ratio. It was observed that the liposomes' drug loading capacity prepared without DSPC was less than 50%. Without DSPC the size of the liposomes was found between 134.0 ± 7.8 and 161.0 ± 9.4 nm for control and 140 ± 9.1 and 177 ± 7.9 nm for PCSK9 conjugated liposomes. Considerable improvement in the drug entrapment and particle size was observed with the introduction of DSPC in the formulation. Liposomes of the size 90.0 ± 4.9–139.0 ± 10.8 nm (Control) and 115.0 ± 4.8–177.0 ± 8.4 nm (PCSK9 conjugated liposome) was obtained with the introduction of DSPC. With DSPC, the drug loading capability of the lipid nanoparticles was also improved from *39–76% for* unconjugated liposomes and 30–71% for conjugated liposomes.

The stability of the lipid nanoparticles was analysed for a period of 30 days. Prepared formulations were stored for thirty days at 4 °C. The change in the physical characters like particle size and PDI was measured after 30 days. No statistically noteworthy alteration in the values was detected as compared to the freshly prepared.

In the present investigation, we used DSP-PEG-2000-COOH to conjugate the PCSK9. PEG-2000 helps to improve the systemic circulation time and passively targets the tumor through the enhanced permeation retention effect. Enhance retention of the liposomes due to the PEG-2000 also improve the therapeutic outcome and, at the same time, decrease the off-site accumulation of cytotoxic drugs. In the present investigation, no significant difference in the entrapment ratio was observed when 2% molar ratio PTX was loaded. As the higher lipid drug ratio may affect the liposomes' stability, 1% PTX molar ratio was finalized.

Overall, in the present investigation, we conjugated LDL receptor-ligand PCSK9 protein to the liposomes. Such liposomes can specifically target the cells expressing higher than the normal levels of LDL receptors e.g., cancer cells. Hence here, we assumed that the PCSK9 conjugated liposomes would reduce the PTX accumulation in the healthy cells and simultaneously exert its anticancer effect on high PCSK9 expressing cells. Also, because of the higher stability, leakage of the PTX in the circulation will be minimum.

In conclusion, the PCSK9 conjugated liposomes could diminish the systemic side effects of PTX. Therefore, such liposomes may help to safely increase the PTX dose whilst limiting the PTX associated side effects. Based on the present results, we conclude that the prepared liposomes are good candidates for transporting PTX to the cancer cells. Hence, in the future, we are considering its evaluation in animal tumor models, followed by its distribution in various tissues and organs.

Conflict of interest statement

All Authors declare No Conflict of Interest.

Data availability

Data will be made available on request.

Acknowledgment

Nitin Bharat Charbe is the recipient of ANID/CONICYT POST-DOCTORADO Fellowship (PROYECTO N° 3180250).

References

[1] W. Xiaoyong, G. Zijian, Targeting and delivery of platinum-based anticancer drugs, Chem. Soc. Rev. 42 (2013) 202–224, https://doi.org/10.1039/c2cs35259a.

[2] C. Carvalho, R. Santos, S. Cardoso, S. Correia, P. Oliveira, M. Santos, P. Moreira, Doxorubicin: the good, the bad and the ugly effect, Curr. Med. Chem. 16 (2009) 3267–3285, https://doi.org/10.2174/092986709788803312.

[3] K. Nurgali, R.T. Jagoe, R. Abalo, Editorial: Adverse effects of cancer chemotherapy: Anything new to improve tolerance and reduce sequelae, Front. Pharmacol. 9 (2018) 245, https://doi.org/10.3389/fphar.2018.00245.

[4] B. Vergès, T. Walter, B. Cariou, Effects of anti-cancer targeted therapies on lipid and glucose metabolism, Eur. J. Endocrinol. 170 (2014) r43–r55, https://doi.org/10.1530/EJE-13-0586.

[5] P. Sapra, T.M. Allen, Ligand-targeted liposomal anticancer drugs, Prog. Lipid Res. 42 (2003) 439–462, https://doi.org/10.1016/S0163-7827(03)00032-8.

[6] K. Cho, X. Wang, S. Nie, Z. Chen, D.M. Shin, Therapeutic nanoparticles for drug delivery in cancer, Clin. Cancer Res. 14 (2008) 1310–1316, https://doi.org/10.1158/1078-0432.CCR-07-1441.

[7] S. Tenzer, D. Docter, J. Kuharev, A. Musyanovych, V. Fetz, R. Hecht, F. Schlenk, D. Fischer, K. Kiouptsi, C. Reinhardt, K. Landfester, H. Schild, M. Maskos, S. K. Knauer, R.H. Stauber, Rapid formation of plasma protein corona critically affects nanoparticle pathophysiology, Nat. Nanotechnol. 8 (2013) 772–781, https://doi.org/10.1038/nnano.2013.181.

[8] P. Aggarwal, J.B. Hall, C.B. McLeland, M.A. Dobrovolskaia, S.E. McNeil, Nanoparticle interaction with plasma proteins as it relates to particle biodistribution, biocompatibility and therapeutic efficacy, Adv. Drug Deliv. Rev. 61 (2009) 428–437, https://doi.org/10.1016/j.addr.2009.03.009.

[9] C. Buzea, I.I. Pacheco, K. Robbie, Nanomaterials and nanoparticles: Sources and toxicity, Biointerphases (2007), https://doi.org/10.1116/1.2815690.

[10] W.J. Stark, Nanoparticles in biological systems, Angew. Chemie - Int. Ed. 50 (2011) 1242–1258. doi:10.1002/anie.200906684.

[11] T. Yang, M.K. Choi, F. De Cui, J.S. Kim, S.J. Chung, C.K. Shim, D.D. Kim, Preparation and evaluation of paclitaxel-loaded PEGylated immunoliposome, J. Control. Release 120 (2007) 169–177, https://doi.org/10.1016/j.jconrel.2007.05.011.

[12] T. Yang, F. De Cui, M.K. Choi, H. Lin, S.J. Chung, C.K. Shim, D.D. Kim, Liposome formulation of paclitaxel with enhanced solubility and stability, Drug Deliv. 14 (2007) 301–308, https://doi.org/10.1080/10717540601098799.

[13] R. Kunstfeld, G. Wickenhauser, U. Michaelis, M. Teifel, W. Umek, K. Naujoks, K. Wolff, P. Petzelbauer, Paclitaxel encapsulated in cationic liposomes diminishes tumor angiogenesis and melanoma growth in a “humanized” SCID mouse model, J. Invest. Dermatol. 120 (2003) 476–482, https://doi.org/10.1046/j.1523-1747.2003.12057.x.

[14] A. Sharma, E. Mayhew, L. Bolcsak, C. Cavanaugh, P. Harmon, A. Janoff, R. J. Bernacki, Activity of paclitaxel liposome formulations against human ovarian tumor xenografts, Int. J. Cancer 71 (1997) 103–107, https://doi.org/10.1002/(SICI)1097-0215(19970328)71:1<103::AID-IJC17>3.0.CO;2-J.

[15] A. Cabanes, K.E. Briggs, P.C. Gokhale, J.A. Treat, A. Rahman, Comparative in vivo studies with paclitaxel and liposome-encapsulated paclitaxel, Int. J. Oncol. 12 (1998) 1035–1040, https://doi.org/10.3892/ijo.12.5.1035.

[16] J.W. Park, Liposome-based drug delivery in breast cancer treatment, Breast Cancer Res 4 (2002) 95–99, https://doi.org/10.1186/bcr432.

[17] J. Lao, J. Madani, T. Puértolas, M. Álvarez, A. Hernández, R. Pazo-Cid, Á. Artal, A. Antón Torres, Liposomal Doxorubicin in the Treatment of Breast Cancer Patients: A Review, J. Drug Deliv. 2013 (2013) 1–12, https://doi.org/10.1155/2013/456409.

[18] A. Nagayasu, K. Uchiyama, H. Kiwada, The size of liposomes: A factor which affects their targeting efficiency to tumors and therapeutic activity of liposomal antitumor drugs, Adv. Drug Deliv. Rev. 40 (1999) 75–87, https://doi.org/10.1016/S0169-409X(99)00041-1.

[19] O. Seifert, N. Pollak, A. Nusser, F. Steiniger, R. Rüger, K. Pfizenmaier, R. E. Kontermann, Immuno-LipoTRAIL: Targeted delivery of TRAIL-functionalized liposomal nanoparticles, Bioconjug. Chem. 25 (2014) 879–887, https://doi.org/10.1021/bc400517j.

[20] M.M. Elmi, M.N. Sarbolouki, A simple method for preparation of immuno-magnetic liposomes, Int. J. Pharm. 215 (2001) 45–50, https://doi.org/10.1016/S0378-5173(00)00667-0.

[21] R. Solaro, F. Chiellini, A. Battisti, Targeted delivery of protein drugs by nanocarriers, Mater. (Basel) 3 (2010) 1928–1980, https://doi.org/10.3390/ma3031928.

[22] G. Storm, M.H. Vingerhoeds, D.J.A. Crommelin, H.J. Haisma, Immunoliposomes bearing enzymes (immuno-enzymosomes) for site-specific activation of anticancer prodrugs, in: Adv. Drug Deliv. Rev., 1997, https://doi.org/10.1016/S0169-409X(96)00461-9.

[23] T.A. Elbayoumi, V.P. Torchilin, Tumor-specific anti-nucleosome antibody improves therapeutic efficacy of doxorubicin-loaded long-circulating liposomes against primary and metastatic tumor in mice, Mol. Pharm. 6 (2009) 246–254, https://doi.org/10.1021/mp8001528.

[24] T.A. Elbayoumi, V.P. Torchilin, Tumor-Targeted immuno-liposomes for delivery of chemotherapeutics and diagnostics, J. Pharm. Innov. 3 (2008) 51–58, https://doi.org/10.1007/s12247-008-9021-7.

[25] Y. Yang, X. Tai, K. Shi, S. Ruan, Y. Qiu, Z. Zhang, B. Xiang, Q. He, A new concept of enhancing immuno-chemotherapeutic effects against B16F10 tumor via systemic administration by taking advantages of the limitation of EPR effect, Theranostics 6 (2016) 2141–2160, https://doi.org/10.7150/thno.16184.

[26] C. Harding, J. Heuser, P. Stahl, Receptor-mediated endocytosis of transferrin and recycling of the transferrin receptor in rat reticulocytes. J. Cell Biol. 97 (1983) 329–339, https://doi.org/10.1083/jcb.97.2.329.

[27] H. Hillaireau, P. Couvreur, Nanocarriers’ entry into the cell: Relevance to drug delivery, Cell. Mol. Life Sci. 66 (2009) 2873–2896, https://doi.org/10.1007/s00018-009-0053-z.

[28] A.A. D’Souza, P.V. Devarajan, Asialoglycoprotein receptor mediated hepatocyte targeting - Strategies and applications, J. Control. Release 203 (2015) 126–139, https://doi.org/10.1016/j.jconrel.2015.02.022.

[29] D. Sun, J. Chen, Y. Wang, H. Ji, R. Peng, L. Jin, W. Wu, Advances in refunctionalization of erythrocyte-based nanomedicine for enhancing cancer-targeted drug delivery, Theranostics 9 (2019) 6885–6900, https://doi.org/10.7150/thno.36510.

[30] S. Ghosh, S. Dutta, A. Sarkar, M. Kundu, P.C. Sil, Targeted delivery of curcumin in breast cancer cells via hyaluronic acid modified mesoporous silica nanoparticle to enhance anticancer efficiency, Colloids Surf. B Biointerfaces 197 (2021), 111404, https://doi.org/10.1016/j.colsurfb.2020.111404.

[31] M. Soleymani, M. Velashjerdi, M. Asgari, Preparation of hyaluronic acid-decorated mixed nanomicelles for targeted delivery of hydrophobic drugs to CD44-overexpressing cancer cells, Int. J. Pharm. 592 (2021), 120052, https://doi.org/10.1016/j.ijpharm.2020.120052.

[32] K. Kucharczyk, A. Florczak, T. Deptuch, K. Penderecka, K. Jastrzebska, A. Mackiewicz, H. Dams-Kozlowska, Drug affinity and targeted delivery: Double functionalization of silk spheres for controlled doxorubicin delivery into Her2-positive cancer cells, J. Nanobiotechnol. 18 (2020), https://doi.org/10.1186/s12951-020-00609-2.

[33] O. Oladimeji, J. Akinyelu, M. Singh, Co-polymer functionalised gold nanoparticles show efficient mitochondrial targeted drug delivery in cervical carcinoma cells, J. Biomed. Nanotechnol. 16 (2020) 853–866, https://doi.org/10.1166/jbn.2020.2930.

[34] C.Y. Wang, B.L. Lin, C.H. Chen, Targeted drug delivery using an aptamer against shared tumor-specific peptide antigen of MAGE-A3, Cancer Biol. Ther. 22 (2021) 12–18, https://doi.org/10.1080/15384047.2020.1833156.

[35] A. Ahmed, S. Sarwar, Y. Hu, M.U. Munir, M.F. Nisar, F. Ikram, A. Asif, S. U. Rahman, A.A. Chaudhry, I.U. Rehman, Surface-modified polymeric nanoparticles for drug delivery to cancer cells, Expert Opin. Drug Deliv. 18 (2021) 1–24, https://doi.org/10.1080/17425247.2020.1822321.

[36] S. Kunjiappan, P. Pavadai, S. Vellaichamy, S. Ram Kumar Pandian, V. Ravishankar, P. Palanisamy, S. Govindaraj, G. Srinivasan, A. Premanand, M. Sankaranarayanan, P. Theivendren, Surface receptor-mediated targeted drug delivery systems for enhanced cancer treatment: A state-of-the-art review, Drug Dev. Res. 82 (2021) 309–340, https://doi.org/10.1002/ddr.21758.

[37] G. Shrivastava, H.A. Bakshi, A.A. Aljabali, V. Mishra, F.L. Hakkim, N.B. Charbe, P. Kesharwani, D.K. Chellappan, K. Dua, M.M. Tambuwala, Nucleic acid aptamers as a potential nucleus targeted drug delivery system, Curr. Drug Deliv. 17 (2020) 101–111, https://doi.org/10.2174/1567201817666200106104332.

[38] L. Persson, G. Cao, L. Ståhle, B.G. Sjöberg, J.S. Troutt, R.J. Konrad, C. Gälman, H. Wallén, M. Eriksson, I. Hafström, S. Lind, M. Dahlin, P. Åmark, B. Angelin, M. Rudling, Circulating proprotein convertase subtilisin kexin type 9 has a diurnal rhythm synchronous with cholesterol synthesis and is reduced by fasting in humans, Arterioscler. Thromb. Vasc. Biol. 30 (2010) 2666–2672, https://doi.org/10.1161/ATVBAHA.110.214130.

[39] N. Scamuffa, F. Calvo, M. Chrétien, N.G. Seidah, A.M. Khatib, Proprotein convertases: Lessons from knockouts, FASEB J. 20 (2006) 1954–1963, https://doi.org/10.1096/fj.05-5491rev.

[40] J.D. Horton, J.C. Cohen, H.H. Hobbs, Molecular biology of PCSK9: its role in LDL metabolism, Trends Biochem. Sci. 32 (2007) 71–77, https://doi.org/10.1016/j.tibs.2006.12.008.

[41] P. Henriksson, S. Ericsson, R. Stege, M. Eriksson, M. Rudling, L. Berglund, B. Angelin, Hypocholesterolaemia and increased elimination of low-density lipoproteins in metastatic cancer of the prostate, Lancet 334 (1989) 1178–1180, https://doi.org/10.1016/S0140-6736(89)91790-X.

[42] J. Liu, A. Xu, K.S.-L. Lam, N.-S. Wong, J. Chen, P.R. Shepherd, Y. Wang, Cholesterol-induced mammary tumorigenesis is enhanced by adiponectin deficiency: role of LDL receptor upregulation, Oncotarget 4 (2013) 1804–1818, https://doi.org/10.18632/oncotarget.1364.

[43] W. Liao, C.H. Florén, Upregulation of low density lipoprotein receptor activity by tumor necrosis factor, a process independent of tumor necrosis factor-induced lipid synthesis and secretion, Lipids 29 (1994) 679–684, https://doi.org/10.1007/BF02538911.

[44] A. Chimento, I. Casaburi, P. Avena, F. Trotta, A. De Luca, V. Rago, V. Pezzi, R. Sirianni, Cholesterol and its metabolites in tumor growth: Therapeutic potential of statins in cancer treatment, Front. Endocrinol. (Lausanne). 10 (2019) 807, https://doi.org/10.3389/fendo.2018.00807.

[45] D. Gal, M. Ohashi, P.C. MacDonald, H.J. Buchsbaum, E.R. Simpson, Low-density lipoprotein as a potential vehicle for chemotherapeutic agents and radionucleotides in the management of gynecologic neoplasms., Am. J. Obstet. Gynecol. 139 (1981) 877–85. http://www.ncbi.nlm.nih.gov/pubmed/7223790 (toegang verkry 22 November 2016).

[46] D. Gal, P.C. Macdonald, J.C. Porter, E.R. Simpson, Cholesterol metabolism in cancer cells in monolayer culture. III. Low-density lipoprotein metabolism, Int. J. Cancer 28 (1981) 315–319, https://doi.org/10.1002/ijc.2910280310.

[47] M.J. Rudling, E. Reihner, K. Einarsson, S. Ewerth, B. Angelin, Low density lipoprotein receptor-binding activity in human tissues: Quantitative importance of hepatic receptors and evidence for regulation of their expression in vivo, Proc.

Natl. Acad. Sci. U. S. A 87 (1990) 3469–3473, https://doi.org/10.1073/pnas.87.9.3469.
[48] M.J. Rudling, B. Angelin, C.O. Peterson, V.P. Collins, Low Density Lipoprotein Receptor Activity in Human Intracranial Tumors and Its Relation to the Cholesterol Requirement, Cancer Res 50 (1990) 483–487. ⟨http://cancerres.aacrjournals.org/content/50/3/483.abstract⟩.
[49] S. Vitols, C. Peterson, O. Larsson, P. Holm, B. Aberg, Elevated uptake of low density lipoproteins by human lung cancer tissue in vivo, Cancer Res 52 (1992) 6244–6247.
[50] G. Norata, G. Canti, L. Ricci, A. Nicolin, E. Trezzi, A.L. Catapano, In vivo assimilation of low density lipoproteins by a fibrosarcoma tumour line in mice, Cancer Lett. 25 (1984) 203–208, https://doi.org/10.1016/S0304-3835(84)80046-4.
[51] M.J. Rudling, L. Ståhle, C.O. Peterson, L. Skoog, Content of low density lipoprotein receptors in breast cancer tissue related to survival of patients, Br. Med. J. (Clin. Res. Ed.). 292 (1986) 580–582. ⟨http://www.ncbi.nlm.nih.gov/pubmed/3081176⟩.
[52] N.G. Seidah, Z. Awan, M. Chrétien, M. Mbikay, PCSK9: A key modulator of cardiovascular health, Circ. Res. 114 (2014) 1022–1036, https://doi.org/10.1161/CIRCRESAHA.114.301621.
[53] R. Hájek, Paclitaxel (Taxol), Cas. Lek. Cesk. 135 (1996) 393–396, https://doi.org/10.1002/j.1875-9114.1994.tb02785.x.
[54] S. Malik, R.M. Cusidó, M.H. Mirjalili, E. Moyano, J. Palazón, M. Bonfill, Production of the anticancer drug taxol in Taxus baccata suspension cultures: A review, Process Biochem 46 (2011) 23–34, https://doi.org/10.1016/j.procbio.2010.09.004.
[55] A. Sparreboom, O. Van Teilingen, W.J. Nooijen, J.H. Beijnen, Nonlinear pharmacokinetics of paclitaxel in mice results from the pharmaceutical vehicle cremophor EL, Cancer Res 56 (1996) 2112–2115.
[56] H. Gelderblom, J. Verweij, K. Nooter, A. Sparreboom, Cremophor EL: The drawbacks and advantages of vehicle selection for drug formulation, Eur. J. Cancer 37 (2001) 1590–1598, https://doi.org/10.1016/S0959-8049(01)00171-X.
[57] D.A. Yardley, Nab-Paclitaxel mechanisms of action and delivery, J. Control. Release 170 (2013) 365–372, https://doi.org/10.1016/j.jconrel.2013.05.041.
[58] N.K. Ibrahim, N. Desai, S. Legha, P. Soon-Shiong, R.L. Theriault, E. Rivera, B. Esmaeli, S.E. Ring, A. Bedikian, G.N. Hortobagyi, J.A. Ellerhorst, Phase I and pharmacokinetic study of ABI-007, a Cremophor-free, protein-stabilized, nanoparticle formulation of paclitaxel, Clin. Cancer Res. 8 (2002) 1038–1044.
[59] S.S. Hong, J.Y. Choi, J.O. Kim, M.K. Lee, S.H. Kim, S.J. Lim, Development of paclitaxel-loaded liposomal nanocarrier stabilized by triglyceride incorporation, Int. J. Nanomed. 11 (2016) 4465–4477, https://doi.org/10.2147/IJN.S113723.
[60] Q. Feng, M.Z. Yu, J.C. Wang, W.J. Hou, L.Y. Gao, X.F. Ma, X.W. Pei, Y.J. Niu, X. Y. Liu, C. Qiu, W.H. Pang, L.L. Du, Q. Zhang, Synergistic inhibition of breast cancer by co-delivery of VEGF siRNA and paclitaxel via vapreotide-modified core-shell nanoparticles, Biomaterials 35 (2014) 5028–5038, https://doi.org/10.1016/j.biomaterials.2014.03.012.
[61] M.L. Immordino, P. Brusa, S. Arpicco, B. Stella, F. Dosio, L. Cattel, Preparation, characterization, cytotoxicity and pharmacokinetics of liposomes containing docetaxel, J. Control. Release 91 (2003) 417–429, https://doi.org/10.1016/S0168-3659(03)00271-2.
[62] P. Crosasso, M. Ceruti, P. Brusa, S. Arpicco, F. Dosio, L. Cattel, Preparation, characterization and properties of sterically stabilized paclitaxel-containing liposomes, J. Control. Release 63 (2000) 19–30, https://doi.org/10.1016/S0168-3659(99)00166-2.
[63] H. Itokawa, K.-H. Lee, Taxus: the genus taxus, Taylor & Francis, 2003.
[64] R.P. Sonali, N. Singh, G. Singh, M.R. Sharma, B. Vijayakumar, S. Koch, U. Singh, D. Singh, B.L. Dash, M.S.Muthu Pandey, Transferrin liposomes of docetaxel for brain-targeted cancer applications: formulation and brain theranostics, Drug Deliv. 23 (2016) 1261–1271, https://doi.org/10.3109/10717544.2016.1162878.
[65] M.S. Muthu, R.V. Kutty, Z. Luo, J. Xie, S.S. Feng, Theranostic vitamin E TPGS micelles of transferrin conjugation for targeted co-delivery of docetaxel and ultra bright gold nanoclusters, Biomaterials 39 (2015) 234–248, https://doi.org/10.1016/j.biomaterials.2014.11.008.